Satellite observations of intense intraseasonal cooling events in the tropical South Indian Ocean.

N. H. Saji, S. -P. Xie and C. -Y. Tam
International Pacific Research Center, University of Hawaii, Honolulu, HI , USA

Intense intraseasonal cooling events in the tropical South Indian Ocean are examined using eight years of TRMM observations. These events occur almost every year during austral summer when the intertropical convergence zone is displaced south of the equator and roughly collocated with a thermocline ridge. Composite maps of SST, OLR and surface winds, based on eleven cooling events with SST exceeding 1^0C, suggest that reduced solar radiation, enhanced evaporation and possibly strong entrainment over the thermocline ridge all play a role in the SST cooling. OLR and covariability in SST exhibit latitudinal variations in spectrum. A distinct southern mode around 10^0S -5^0S exhibits a peak in coherence-squared at a period of 65 days. In contrast, an equatorially symmetric mode has a coherence-squared peak at 35 days. This may hint at a possible feedback onto the atmosphere from strong intraseasonal SST variability over the South Indian Ocean.

1 Introduction

Intense cooling in sea surface temperature (SST) on intraseasonal timescales have been recently reported in the south Indian Ocean during austral summer [Harrison and Vecchi, 2001; Duvel et al., 2004]. The magnitude of the SST cooling during these events (O$\approx$ 1^0 C) is unexpectedly large in comparison to earlier estimates of 0.15 to 0.3^0 C [Kawamura, 1988; Shinoda et al., 1998; Zhang and McPhaden, 2000] over the Indo-Pacific warm pool. The detection of these events is made possible by the introduction of microwave remote sensing [Wentz et al., 2000] in December 1997 on the Tropical Rain Measuring Mission (TRMM) satellite that allowed the retrieval of SST through clouds.

Harrison and Vecchi [2001] and Duvel et al. [2004] discussed two particular events during January and March 1999 in which SST dropped by as much as 3^0C. The strongest cooling during these events took place in the southwest tropical Indian Ocean, whereas earlier studies had noted that the strongest SST variability in conjunction with the Madden-Julian Oscillation (MJO) occurs over the Indonesian region [Shinoda et al., 1998, for e.g]. The extraordinary strength and unusual spatial structure of SST variability during these two events raise many important questions: Are these cooling events unique to the year of 1999 or are they a common feature of SST variability in the Indian Ocean missed by inadequate observations? Which season do these cooling events favor and do they share some common characteristics in space and time? The present study addresses these questions by using eight years of satellite microwave measurements of SST. Our analysis shows that strong cooling events like the one described by Harrison and Vecchi [2001] commonly occurs in the tropical South Indian Ocean, observed almost every year from November to April when the marine inter-tropical convergence zone (ITCZ) moves south of the equator and the MJO is active and propagates eastward along the equator [Madden and Julian, 1994]. To our knowledge, this is the first study that composites a large number of cooling events to isolate their common space-time structures, a first step toward understanding their dynamics. Our results show that these SST events are associated with large-scale, organized anomalies of atmospheric convection and surface wind. Section 2 briefly describes the data and Section 3 presents the statistical analysis. Section 4 summarizes the results and discusses possible SST feedback onto atmospheric variability.

2 Data and Methods

We used the Level 3 TRMM Microwave Imager (TMI) product for SST(http://www.remss.com) and vector surface winds from the SeaWinds sccatterometer on the QuikSCAT satellite [Liu et al., 2000]. TMI and QuikSCAT data, originally on a 0.25 x 0.25 degree grid, were binned into 2.5 by 2.5^0 boxes and data gaps filled using linear spatial and time interpolation. As a measure of deep convection, daily interpolated 2.5^0 by 2.5^0 NOAA Out-

going Longwave Radiation (OLR) was used. We used the above data at daily resolution for the period from 06 Dec 1997 to 31 Aug 2005, except for QuickSCAT wind available only from 15 July 1999. A 20-200 day Lanczos band-pass filter with 241 weights, as discussed in Matthews [2000], was used to isolate intraseasonal variability (ISV). The use of this rather wide bandwidth (compared to the common usage of 30-90 day bandpassing) avoids the undesirable possibility of successive intraseasonal events being artificially smeared into each other [Matthews, 2000]. We note, however, that the results of this analysis do not change even if we use a narrower (30-90 day) bandpassing. The spectral analysis, however, was conducted using unfiltered data (see 'auxiliary material' for further details).

3 Results

We have computed the standard deviation of ISV in SST, wind speed and OLR for four seasons. Three regions of high SST variance stand out. One is in austral summer over the tropical South Indian Ocean (Fig. 1) while the rest are both in boreal summer, in the western Arabian Sea and Bay of Bengal, respectively (not shown). In the summer western Arabian Sea, SST variability is dominated by eddies in the Somali current system and cold upwelling filaments[Vecchi et al., 2004] while wind speed and OLR variability is weak. In the Bay of Bengal, large instraseasonal SST anomalies are associated with boreal summer ISV [Sengupta et al., 2001b]. Coupled model experiments suggest that the SST variability provides important feedbacks to atmospheric ISV, especially its northward propagating component [Fu et al., 2003].

Figure 1 shows the intraseasonal standard deviations of SST, wind speed and OLR during austral summer (December-February). This study focuses on the high SST variance that spans the entire Indian Ocean in the zonal direction and is meridionally confined between 10^0 S and 5^0 S. The standard deviations exceed 0.6^0 C in the western two-thirds of the region, but individual events can produce peak to trough drops of as much as 3^0 C in total SST (Fig. 2b). In the tropical South Indian Ocean, the SST variance peaks in austral summer and decreases by a factor of 2 in other seasons (not shown). These strong SST variations occur directly beneath the austral summer intertropical convergence zone (ITCZ) and are coincident with regions of strong ISV in wind speed and OLR (white contours in Fig. 1). The spatial patterns of wind speed and OLR variance, however, do not fully account for the spatial structure of SST variability. In particular, the former two fields have broader meridional extents than SST, especially in the eastern basin. Further, while wind speed and OLR variance increases eastward, SST variance increases westward instead. All this suggests influences of subsurface ocean structures. In particular, a thermocline ridge [Xie et al., 2002] is roughly collocated with the high SST variance (Fig. 1). Forced by the mean Ekman pumping under the southward-displaced Indian Ocean ITCZ, the thermocline in the ridge shoals toward the west, helping enhance SST variability in the western basin in response to atmospheric forcing.

Figure 2a displays the longitude-time section of filtered SST anomalies averaged in 5-10^0S (for clarity only 3 years of data are shown). During each austral summer, zonally coherent anomalies of the basin scale develop and decay several times. These austral-summer anomalies display little zonal propagation. In other seasons, by contrast, this nearly

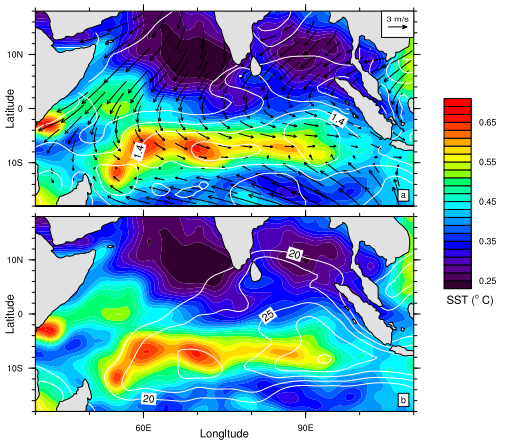

Figure 1 a) Standard deviation of intraseasonal SST (shaded, in ^{0} C) and wind speed (contour, in m/s) anomalies during DJF. b) Same as a), but the contours are for standard deviation of intraseasonal OLR anomalies in W/m^2. Vectors in a) depict the climatological surface winds during DJF.

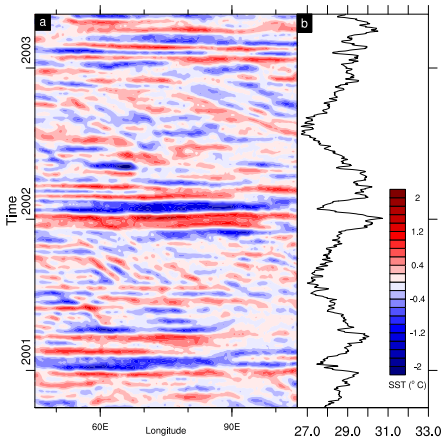

Figure 2 a) Longitude-time plot of intraseasonal SST anomaly (^{0} C) averaged between 10^0S and 5^0S. b) Time series of area-averaged unfiltered SST from 60^0-90^0E and 10^0-5^0S.

zonally uniform feature is replaced by SST anomalies of shorter zonal scales that display clear westward propagation. These smaller-scale, propagating features in SST are likely due to the advection of mean SST gradients by ocean Rossby waves [Small et al., 2005]. Significant northward SST gradients develop in this region in seasons other than austral summer. During the austral summer, mean SST gradients weaken, allowing other mechanisms to dominate intraseasonal SST variability.

The intensity and spatial coherence of SST cooling events in austral summer are so striking that they can be identified even from unfiltered data. Fig. 2b illustrates this with a time series of unfiltered TMI SST averaged over 60^0E to 90^0E and 10^0S to 5^0S. Subseasonal variations of SST are readily seen, punctuating the annual rise of SST from austral winter to summer. The most pronounced cooling event in the TMI data set took place in January 2002, in which SST dropped from 30.5^0C to 27.5^0C in about 25 days and came back to 30^0C a month later. The amplitude of such cold intraseasonal anomalies is comparable to the seasonal change from winter to summer in an average year.

To map the structure of intraseasonal cold events and their relationship with atmospheric variability, we performed a composite analysis of OLR, wind and SST with respect to a band passed version of the area-mean SST index shown in Fig. 2b. We also performed an EOF analysis of intraseasonal SST variability and the first principal component for austral summer is highly correlated with this index. Eleven austral summer cool events (Table 1) during the period 1998 to 2005 were selected when the band passed index showed negative anomalies exceeding 1.5 standard deviations between November and March. Figure 3 shows the composites at four phases corresponding to the initiation (lag=-90^0), growth (lag=-45^0), peak (lag=0^0) and decay (lag=45^0) of the cold SST anomaly. A phase difference of 45^0 is equivalent nominally to a time difference of 7 to 10 days.

27 Jan 1999
24 Mar 1999
04 Jan 2000
25 Feb 2000
23 Jan 2001
29 Nov 2001
27 Jan 2002
07 Feb 2003
14 Nov 2003
30 Dec 2003
10 Mar 2004

Table 1 Dates of peak cool SST anomaly for the 11 events used in the composite analysis

At the initiation phase (lag=-90^0), there are well-developed negative OLR anomalies over the tropical South Indian Ocean, with an cyclonic circulation over and slightly south of the convective anomaly pattern. As part of the cyclonic circulation, considerable westerly wind anomalies develop on the western half of the OLR anomalies. At the growth phase (lag=-45^0), SST cooling intensifies rapidly while OLR anomalies strengthen slightly. At the peak phase (lag=0), large SST anomalies of 0.7^0C are found in a large zonal span of 55-95^0E. Convective anomalies dissipate and move eastward, while large westerly anomalies of 3 m/s appear in the eastern basin. At the decay phase (lag=45^0), SST anomalies begin to dissipate while OLR anomalies turn positive from the equator to 10^0S. Further to the south, there are some remnants of negative OLR anomalies accompanied by a cyclonic wind circulation.

Without in-situ observations, we are unable to de-

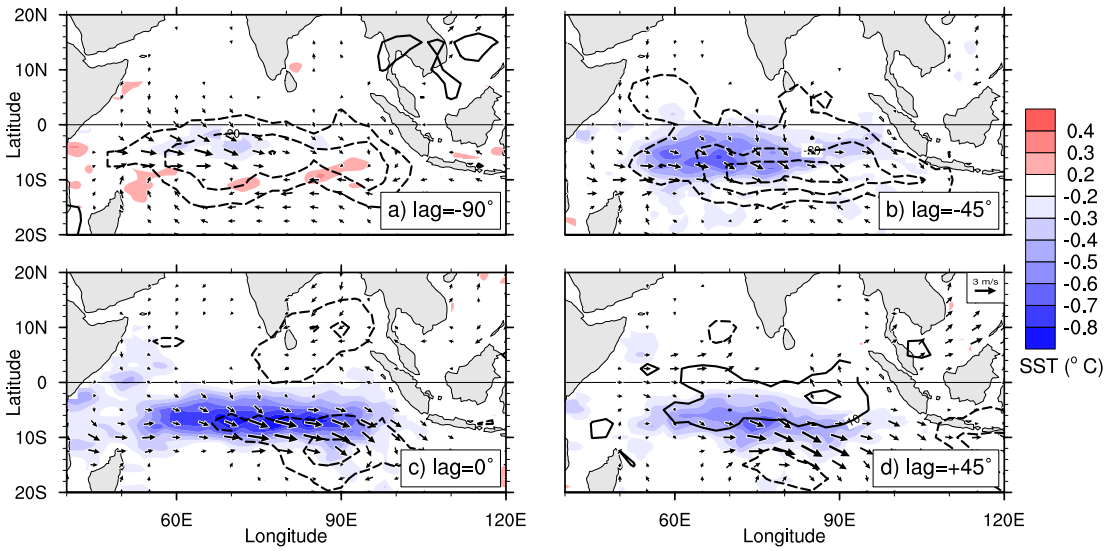

Figure 3 Composite maps of intraseasonal anomalies of SST (shaded, in ^{0} C), OLR (contour, in W/m^2) and surface wind vector (arrows, in m/s) based on 11 austral summer SST cooling events in the south equatorial Indian Ocean. Panels *a* to *d* depict four different phases corresponding to the initiation, growth, peak and decay of SST anomalies

termine the mechanisms for the SST cooling in the South Indian Ocean but the following inferences may be made. First, increased convective activity prior and during the cooling reduces solar radiation and SST. Second, westerly wind anomalies increase wind speed, surface evaporation, and possibly entrainment across the shallow mixed layer over the thermocline ridge. Local Ekman pumping, however, does not seem to be a major player [Waliser et al., 2003]; with the maximum wind anomalies over and slightly south of the maximum SST cooling, wind curl anomalies are nearly 90^0 out of phase with those of SST.

4 Discussion

Active convection and thick clouds are often present over the South Indian Ocean, limiting the ability of infrared sensors to observe the air-sea interface from space. We have taken advantage of cloud-penetrating microwave observations from space that have accumulated for the past eight years and found large intraseasonal SST variability during austral summer over the tropical South Indian Ocean. It has a standard deviation of 0.6^0C with many cooling events exceeding 1 to 2^0C. This is much larger than the typical amplitude of 0.15^0C to 0.3^0C previously reported based on pre-TRMM observations [Kawamura, 1988; Shinoda et al., 1998; Jones et al., 1998]. These intraseasonal cooling events are of the basin scale and associated with well organized atmospheric anomalies. Enhanced convection lead SST anomalies by 7-10 days while surface westerly wind anomalies are nearly in phase, suggesting that both cloud effect on surface solar radiation and wind effect on turbulent heat flux and ocean mixing are important mechanisms for SST anomalies. The climatological thermocline dome in 5-10^0S is probably important for enhanced ISV in SST in the South Indian Ocean, in particular in the western basin where the 20^0C isotherm is only about 80 m deep, about 40m shallower than in the adjacent areas [Xie et al., 2002].

Why then is the austral summer favored for large ISV in SST over the South Indian Ocean? We suggest that the seasonal migration of the ITCZ is the key. During austral summer, the ITCZ reaches its southernmost position roughly collocated with the thermocline dome. Increased convective activity in the ITCZ and the shallow depth of the ocean mixed layer both help enhance SST variability. Austral

summer is also the season when the climatological mean winds are westerly over the thermocline dome (Fig. 1). Generally associated with increased convection, westerly wind anomalies reinforce the cloud cooling effect by intensifying the mean westerlies. We note that the mean westerly winds themselves are due to the southward migration of the ITCZ as the Coriolis force turns the northerly cross-equatorial wind eastward. The collocation of the ITCZ and thermocline ridge as well as large variability in cloud and wind all contribute to high SST variability in the south Indian Ocean during austral summer. This is somewhat similar to the boreal summer Bay of Bengal, where the shallow pycnocline serves a similar role[Sengupta et al., 2001b] as the thermocline ridge in the South Indian Ocean in reducing the mixed layer thermal inertia.

The collocation of the ITCZ and large ISV in SST over the (austral) summer South Indian Ocean raises an interesting question of whether SST anomalies feedback onto atmospheric ISV. The phase lead of convective anomalies suggests atmospheric forcing of the ocean but does not rule out the possibility of oceanic feedback, as is demonstrated for boreal summer ISV over the Bay of Bengal [Fu et al., 2003]. We have computed the auto spectrum of OLR and its co-spectrum with SST as a function of latitude and period, both averaged in 60-90^{0}E (Fig. 4). The spectral calculations were performed using the entire 2824 days of data. To highlight austral summer variability, the time series was multiplied with a masking function [Hartmann and Gross, 1988] that has a value of one during December-February and gradually tapers to zero away from it. After accounting for tapering and smoothing, the resulting spectra in Fig. 4 has 11 effective Degrees of Freedom and a bandwidth of 0.0031 cpd (for more details see 'auxiliary material'). Widening the window to November to March does not change the results.

The OLR auto-spectrum (black contours) suggests that MJO variability may consist of two modes. In a 30-50 day band MJO variability is symmetric about the equator with strongest power within 6^{0}S - 6^{0}N. However, at a lower frequency band between 50 and 70 days, the spectrum is quite asymmetric with strongest power between 12^{0}S and the equator. Hovmoeller and composite analysis (not shown) applied separately to the two frequency bands further suggest that the symmetric mode of OLR variability, while exhibiting a pronounced eastward propagation, dissipates rapidly once it reaches the maritime continent. On the other hand, the southern mode shows slower eastward propagation that extends farther into the western Pacific without significant loss of power at the maritime continent. The most tantalizing aspect of Fig. 4 is that the southern mode of OLR variability shows a high coherence with SST (shading). This may be simply because the ocean responds more readily to lower-frequency variability [Han, 2005], acting as a low-frequency filter of atmospheric variability. An alternative interpretation is that the distinctly lower frequencies of the southern mode and its higher SST co-variability is a manifestation of ocean-atmosphere interaction.

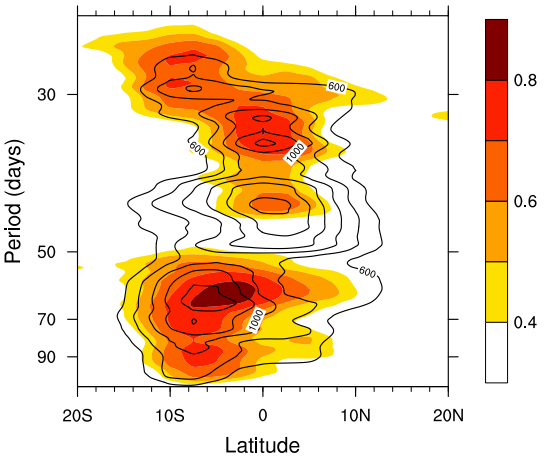

Figure 4 Distribution of SST-OLR coherence squared (shaded) and OLR auto power spectrum (W^2m^{-4}) as a function of latitude and frequency for data averaged between 60^0 to 90^0 E during DJF.

Acknowledgements We thank Jan Hafner for preparing and making available the satellite wind and SST data and Drs. Y. Kuroda, Y. Masumoto, H. Sasaki, H. Hase, and M. Nonaka for valuable discussions. This work is supported by JAMSTEC and NASA. SPX carried out part of the work while on a Japan Society for Promotion of Science visiting fellowship. He wishes to thank Y. Tanimoto, H. Tokinaga and colleagues at Hokkaido University for their hospitality and assistance. This is IPRC contribution 397 and SOEST contribution 6808.

References

[1] D. E. Harrison and G. A. Vecchi, *January 1999 indian ocean cooling event*, Geophys. Res. Lett. **28** (2001), 3717-3720

[2] J. P. Duvel, R. Roca, and J. Vialard, *Ocean mixed layer temperature variations induced by intraseasonal convective perturbations over the indian ocean*, J. Atmos. Sci. **61** (2004), 1004-1023

[3] R. Kawamura, *Intraseasonal variability of sea surface temperature over the tropical western pacific*, J. Meteor. Soc. Japan **66** (1988), 1007-1012

[4] T. Shinoda, H. Hendon, and J. Glick, *Intraseasonal variability of surface fluxes and sea surface temperature in the tropical western pacific and indian oceans*, J. Climate **11** (1998), 1685-1702

[5] C. D. Zhang and M. J. McPhaden, *Intraseasonal surface cooling in the equatorial western pacific*, J. Climate **13** (2000), 2261-2276

[6] F. J. Wentz, C. Gentemann, D. Smith, and D. Chelton, *Satellite measurements of sea surface temperature through clouds*, Science **288** (2000), 847-850

[7] R. Madden and P. Julian, *Observations of the 40-50 day tropical oscillation: a review*, Mon. Wea. Rev. **122** (1994), 814-837

[8] W. T. Liu *et al.*, *Atmospheric manifestation of tropical instability wave observed by quikscat and tropical rain measuring mission*, Geophys. Res. Lett. **27** (2000), 2545-2548

[9] A. J. Matthews, *Propagation mechanisms for the madden-julian oscillation*, Quart. J. Roy. Met. Soc. **126** (2000), 2637-2652

[10] G. A. Vecchi, S.-P. Xie, and A. Fischer, *Ocean-atmosphere covariability in the western arabian sea*, J. Climate **17** (2004), 1213-1224

[11] D. Sengupta, B. N. Goswami, and R. Senan, *Coherent intraseasonal oscillations of ocean and atmosphere during the asian summer monsoon*, Geophys. Res. Lett. **28** (2001), 4127-4130

[12] X. Fu, B. Wang, T. Li, and J. P. McCreary, *Coupling between northward-propagating, intraseasonal oscillations and sea surface temperature in the indian ocean*, J. Atmos. Sci. **60** (2003), 1733-1753

[13] S.-P. Xie, H. Annamalai, F. A. Schott, and J. P. McCreary, *Structure and mechanisms of south indian ocean climate variability*, J. Climate **15** (2002), 864-878

[14] R. J. Small, S.-P. Xie, and J. Hafner, *Satellite observations of mesoscale ocean features and co-propagating atmospheric surface fields in the tropical belt*, J. Geophys. Res. **110** (2005), doi: 10.1029/2004JC002598

[15] D. E. Waliser, R. Murtugudde, and L. E. Lucas, *Indo-pacific ocean response to atmospheric intraseasonal variability: 1. austral summer and the madden-julian oscillation*, J. Geophys. Res. **108** (2003), doi:10.1029/2002JC001620

[16] C. Jones, D. E. Waliser, and C. Gautier, *The influence of the madden-julian oscillation on ocean surface heat fluxes and sea surface temperature*, J. Climate **11** (1998), 1057-1072

[17] D. L. Hartmann and J. R. Gross, *Seasonal variability of the 40-50 day oscillation in wind and rainfall in the tropics*, J. Atmos. Sci. **45** (1988), 2680–2702

[18] W. Han, *Origins and dynamics of the 90-day and 30-60 day variations in the equatorial indian ocean*, J. Phys. Oceanogr. **35** (2005), 708-728

A Electronic Supplement

A.1 Spectral Calculations

A.1.1 Pre-processing of data

The data for spectral analysis was prepared as follows. A mean annual cycle was determined by computing an average for each of the 365 days of the year from the nearly 8 years of data (29 February of leap years was ignored). This composite annual cycle was subjected to harmonic analysis. A smoothed mean annual cycle was then formed from the first 3 harmonics. This was then removed from the original time series and the resulting anomaly time series subjected to spectral analysis.

A.1.2 Determination of seasonal spectra: masking

For the spectral analysis shown in Fig. 4 of the manuscript, the whole time series (from 06 Dec 1997 to 31 Aug 2005) was used. This gives a bandwidth of 1/2824 cpd=.000354cpd. To highlight winter variability, the time series was multiplied with a masking function [Hartmann and Gross, 1988] of the form shown in Fig. 1. The masking function weights the time series unequally. Weights of unit value are used only for the December-January-February sea-

son. From the end of February of a particular year, the weights begin decreasing to zero at 15 July of the same year, in the form of a cosine bell as shown in Fig. 1. After 15 July, the weights increase from zero, again following a cosine bell, and reaches a value of one on 01 December. This manner of determining seasonal spectra ensures that the original bandwidth is not sacrificed. To check the sensitivity of the results to the form of the mask function, the shape of the function was altered by letting the weights taper more rapidly (short dashed line) towards zero. In another test, the window of unit weights was widened to November to March (long dashed line). Both of these masking functions produced the same results as the original mask.

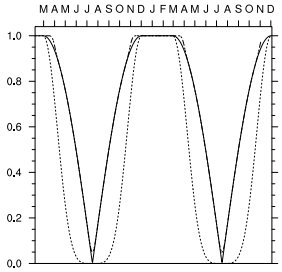

Figure A.1 Masking function

A.1.3 Degrees of Freedom

The degrees of Freedom (DOF) of the spectra shown in Fig. 4 are affected by several factors, including the tapering window used for masking. To ensure the stability of the spectra, 9 adjacent frequency bins were averaged using a Daniell window. The form of the Daniell window (g_i of width m) is given by

$$g_i = \frac{1}{2(m-1)}, i = 1 \; or \; i = m \qquad (A.1)$$

$$= \frac{1}{(m-1)}, i = 2, m-1 \qquad (A.2)$$

The averaging across the frequency band should have yielded 18 Degrees of Freedom (DOF), but for loss of DOF due to zero-padding and the windowing procedures. The increase in variance (equivalently, loss of DOF) of the spectral estimate due to the split cosine-bell taper, given the total proportion of the time series tapered p (=0.66 in this case) is

$$C_{tap} = \frac{128 - 93p}{2 * (8 - 5p)^2} \qquad (A.3)$$

The effective degrees of freedom (EDOF) taking into account increase of variance due to tapering is given by

$$\nu = 2/g_\star^2 \qquad (A.4)$$

where

$$g_\star^2 = C_{tap} \Sigma g_i^2 \qquad (A.5)$$

g_i being the weights associated with the Daniell filter.
The EDOF for our case is thus 11.